A Pneumatically Driven Stewart Platform Used as Fault Detection Device

Martin Ramsauer[1,a] , Michael Kastner[1,b] , Paolo Ferrara[2,c] , Ronald Naderer[2,d] , Hubert Gattringer[1,e]

[1]Institute for Robotics,Johannes Kepler University Linz, Altenbergerstr. 69, 4040 Linz, Austria

[2]FerRobotics Compliant Robot Technology GmbH, Altenbergerstr. 69, 4040 Linz, Austria

[a]martin.ramsauer@jku.at, [b]michael.kastner@jku.at, [c]paolo.ferrara@ferrobotics.at, [d]ronald.naderer@ferrobotics.at, [e]hubert.gattringer@jku.at,

Keywords: Stewart Platform, Hexapod, Fault Detection, Pneumatic Artificial Muscle, Robotics, Control, Simulation, Equation of Motion.

Abstract. This paper investigates the sensorless detection and evaluation of inner oscillations of unknown test objects mounted on a compliant test bench. The principle of the sensorless analysis is that test objects are not totally rigid in reality. This means one or more parts of the test objects are oscillating with different eigenfrequencies compared to their rigid equivalent. By comparing eigenfrequencies of both (rigid and fault test object) oscillating parts are detectable.

The aim of this experiment is to demonstrate the use of a 6 DOF compliant Stewart platform (alternatively used in a simulation environment) to generate frequency sweeps in all degrees of freedom, to get a sensorless detection of vibrations in unknown objects. For this purpose only the preexisting sensors applied for the control of the hexapod should be used.

The detection of loose parts by shaking objects can be done by a complex robotic manipulation task. Being designed for flexible use by small and medium-sized enterprises, the robotic Stewart platform (hexapod) will adapt autonomously to different test objects leading to a highly flexible robot.

Introduction

Countless everyday life products such as electronic equipment or complex parts of the automobile industry suffer from mechanical strain like vibration or shock. The product design has to take all these stress factors into account to guarantee the full function of a product during shipping and final use. It is indispensable to test and measure all these stress factors beforehand. Usually these sorts of vibration tests are carried out on special vibrating units or shaking platforms. Electric shakers are being used mainly for higher vibration frequencies in one dimension. To test for more complex movements, hydraulic multi axes motion units are commonly used, each custom built for a specific vibration pattern. To overcome this drawback one could use a Stewart platform instead, which is capable of complex movements in all 6 degrees of freedom and is easy to reconfigure. If a different pattern is needed one has only to change the trajectory of the hexapod.

Design

In general a hexapod consists of a base and a moving plate connected by 6 actuators that are capable of generating push and pull forces [4]. A recent realization at FerRobotics Compliant Robot Technology GmbH from Linz (Austria) uses pneumatic muscles, which are only able to produce contraction forces, thus it would not be possible to apply a load. To compensate this, a centered spring for expansion forces is integrated in the design of the muscle hexapod [7]. The spring is highly nonlinear and not well specified. But the given design is light weight, easy to transport and environmentally safe. The aim of the project is to determine if a test load put on the hexapod changes in behavior i.e. to sens if something gets loose or even breaks without additional sensors. The test load has to undergo a specific trajectory, following high accelerations and extensive vibrations. Given all these constraints

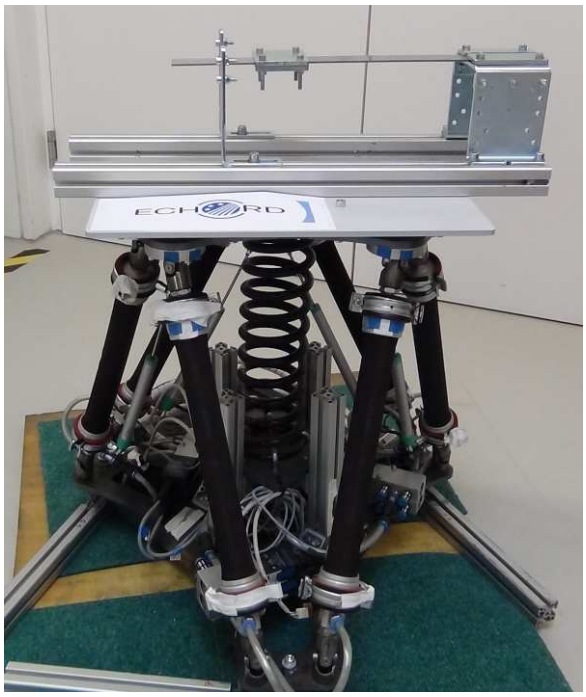

Fig. 1: Picture of the hexapod layout with test load

it should be possible to observe a change in the load structure by using the preexisting sensors applied for the control of the hexapod. It is crucial to derive a perfect mathematical model of the hexapod to accomplish this. The proposed load model consists of two interconnected bodies. This connection is modeled by a damped spring described by a stiffness matrix $\mathbf{K} \in \mathbb{R}^{6,6}$ and a corresponding damping matrix.

Kinematics

In opposite to serial robots, the inverse kinematics for parallel robots can be calculated rather easily, whereas the forward kinematics is more difficult, see [2], [8] and [9].

Inverse Kinematics The inverse kinematics calculates the length of each hexapod leg starting with the known vector $\mathbf{r}_{OP}$ and the orientation $\mathbf{A}_{IK}$. Following the closed vector loop in Fig. 2, each length can be calculated to

$$
\begin{aligned}
{}_I\mathbf{l}_i &= {}_I\mathbf{r}_{OP} + \mathbf{A}_{IK}({}_K\mathbf{b}_i - {}_K\mathbf{r}_{AP}) - {}_I\mathbf{a}_i, && (1)\\
l_i &= \sqrt{{}_I\mathbf{l}_i^T \; {}_I\mathbf{l}_i} \qquad i = 1..6. && (2)
\end{aligned}
$$

Vector ${}_I\mathbf{r}_{OP}$ is the desired position of point P the TCP (Tool Center Point) and ${}_K\mathbf{b}_i$ and ${}_I\mathbf{a}_i$ are given by the design of the robot. The rotation matrix is calculated by using Cardan angles to

$$
\mathbf{A}_{IK} = \mathbf{A}_{KI}^T = (\mathbf{A}_\gamma \mathbf{A}_\beta \mathbf{A}_\alpha)^T. \qquad (3)
$$

The inverse kinematics can be calculated with this known information.

Forward Kinematics The position and orientation of point P (TCP) is calculated depending on the robots leg length l_i. This is, however, hard to accomplish in an analytical way, thus a numerical solution is preferred for the real time computation. A set of constraint equations ϕ_i including the inverse kinematics

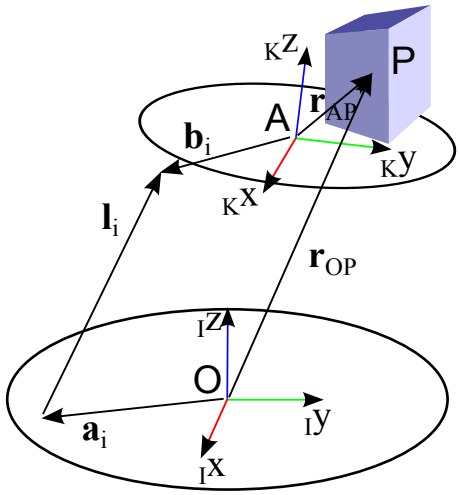

Fig. 2: Layout of a hexapod leg $\mathbf{l}_i$

$$\boldsymbol{\phi} = \begin{pmatrix} \phi_1 & .. & \phi_6 \end{pmatrix}^T, \quad \phi_i = l_i|_{\mathbf{q}^{(n)}} - l_{i,d} = 0, \quad i = 1..6, \tag{4}$$

where $l_{i,d}$ is the set point of leg i leads to the following iteration scheme (Newton-Raphson)

$$\mathbf{q}^{(n+1)} = \mathbf{q}^{(n)} - \underbrace{\boldsymbol{\phi}'|^{-1}_{\mathbf{q}^{(n)}} \, \boldsymbol{\phi}|_{\mathbf{q}^{(n)}}}_{\boldsymbol{\delta}^{(n)}}. \tag{5}$$

The new solution of the $(n+1)$th iteration is $\mathbf{q}^{(n+1)}$ with the Jacobian $\boldsymbol{\phi}' = \partial\boldsymbol{\phi}/\partial\mathbf{q}$ and $\boldsymbol{\delta}$ represents the Newton direction. Due to minimal change in position from one to another step, the starting position of every step is very close to the solution and only 2 iterations per cycle are necessary to obtain a satisfying result.

Dynamics

The dynamical model is derived using the Projection Equation, see [3] for details. The minimal coordinates for the kinematic and dynamic model of the robot are described by the vector $\mathbf{q}^T = (x \;\; y \;\; z \;\; \alpha \;\; \beta \;\; \gamma)$, which represents the tool center point (TCP). The vector $\mathbf{r}^T_{OP} = (x \;\; y \;\; z)$ shows the position and vector $\boldsymbol{\varphi}^T_{OP} = (\alpha \;\; \beta \;\; \gamma)$ the according orientation in Cardan angles.

The linear momentum $\mathbf{p} = m \;\; \mathbf{v}_c$ and angular momentum $\mathbf{L} = \mathbf{J} \;\; \omega_c$ are projected into the minimal space (minimal velocities $\dot{\mathbf{q}}$) via the corresponding Jacobian

$$\sum_{i=1}^{N} \left(\left(\frac{\partial_R \mathbf{v}_c}{\partial \dot{\mathbf{q}}} \right)^T \left(\frac{\partial_R \boldsymbol{\omega}_c}{\partial \dot{\mathbf{q}}} \right)^T \right) \begin{pmatrix} {}_R\dot{\mathbf{p}} + {}_R\,\widetilde{\boldsymbol{\omega}}_{IR} \;\; {}_R\mathbf{p} - {}_R\,\mathbf{f}^e \\ {}_R\dot{\mathbf{L}} + {}_R\,\widetilde{\boldsymbol{\omega}}_{IR} \;\; {}_R\mathbf{L} - {}_R\,\mathbf{M}^e \end{pmatrix}_i = \mathbf{Q}, \tag{6}$$

The translational velocity $\mathbf{v}_c$ as well as the rotational velocity of the center of gravity $\boldsymbol{\omega}_c$ can be inserted in arbitrary coordinate systems R. In contrast to $\boldsymbol{\omega}_c$, $\boldsymbol{\omega}_{IR}$ is the angular velocity of the used reference system. The matrix $\mathbf{J}$ is the inertial tensor, while $\widetilde{\boldsymbol{\omega}} \;\; \mathbf{p}$ characterizes the vector product $\boldsymbol{\omega} \times \mathbf{p}$. $\mathbf{f}^e_i$ and $\mathbf{M}^e_i$ are the impressed forces and moments acting on the ith body. To obtain the actuator (muscle) forces the principle of virtual work is used

$$\delta W = \delta \mathbf{q}^T \mathbf{Q} = \sum \delta \, {}_I\mathbf{r}_i^T \, {}_I\mathbf{F}_i = \sum \delta \mathbf{q}^T \left(\frac{\partial {}_I\mathbf{r}_i}{\partial \mathbf{q}} \right)^T {}_I\mathbf{F}_i, \tag{7}$$

with

$${}_I\mathbf{F}_i = F_i \frac{{}_I\mathbf{l}_i}{\| {}_I\mathbf{l}_i \|}, \tag{8}$$

where F_i is the force of the ith muscle, while ${}_I\mathbf{l}_i / \| {}_I\mathbf{l}_i \|$ represents the normalized direction, see Eq.1. The center spring force is calculated by the potential function

$$V = \frac{1}{2} \mathbf{q}^T \mathbf{K} \mathbf{q}, \tag{9}$$

using the stiffness matrix $\mathbf{K}$ inserted to the equation of motion. Using this potential as part of the generalized force results in

$$\mathbf{Q} = - \left(\frac{\partial V}{\partial \mathbf{q}} \right)^T = -\mathbf{K}\mathbf{q}. \tag{10}$$

The load model consists of two separate bodies which have their center of gravity in points P and B. The first body P is connected with the plate and has no relative movement. The second body

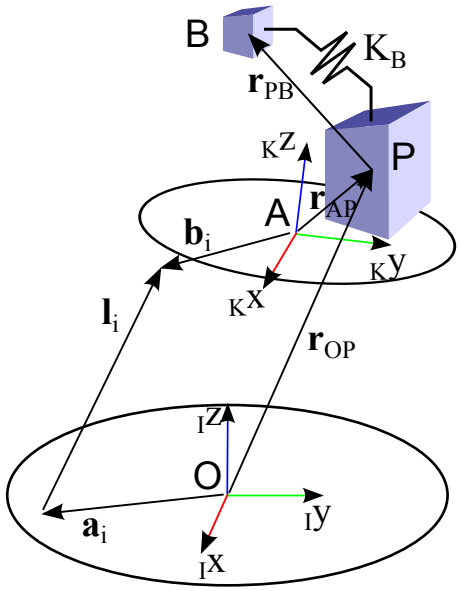

Fig. 3: Load model

is connected by a stiffness matrix $\mathbf{K}_B \in \mathbb{R}^{6,6}$ to the first body. This stiffness matrix is changed during testing. At the beginning of the test parts P and B are connected stiffly, one can say they act as one compact mass. After a while something gets loose and some entries of the stiffness matrix change to describe the loose part. Depending on the desired load model only specific entries can change. To address boundary conditions the matrix entries can change depending on the state vector position and orientation of body B. To implement the relative movement between P and B a second independent body is added to the equation of motion Eq.6 and thus the dimension of $\mathbf{q}$ doubles to $\mathbf{q}^T = (x \;\; y \;\; z \;\; \alpha \;\; \beta \;\; \gamma \;\; u \;\; v \;\; w \;\; \vartheta \;\; \rho \;\; \varphi)$. Where $\mathbf{r}_{PB}^T = (u \;\; v \;\; w)$ represents the position vector from P to B and $\boldsymbol{\gamma}_{PB}^T = (\vartheta \;\; \rho \;\; \varphi)$ the Cardan orientation from K- to B-system. To get a more realistic

behavior of body B, a damping function is added to the equation of motion Eq.6. It is derived by the Rayleigh function, [3] as

$$R_B = \frac{1}{2}\left(d_{t,xy}\left(\dot{u}^2 + \dot{v}^2\right) + d_{t,z}\dot{w}^2 + d_{r,xy}\left(\dot{\vartheta}^2 + \dot{\rho}^2\right) + d_{r,z}\dot{\varphi}^2\right) \tag{11}$$

to

$$\mathbf{Q} = -\left(\frac{\partial R_B}{\partial \dot{\mathbf{q}}}\right)^T. \tag{12}$$

By using Eq.6 - Eq.12 one can obtain the overall equation of motion as follows

$$\mathbf{M}\left(\mathbf{q}\right)\ddot{\mathbf{q}} + \mathbf{g}\left(\mathbf{q}, \dot{\mathbf{q}}\right) + \mathbf{K}\mathbf{q} = \mathbf{B}\left(\mathbf{q}\right)\mathbf{u}, \tag{13}$$

using the 6 muscle forces $\mathbf{u} = \begin{pmatrix} F_1 & .. & F_6 \end{pmatrix}^T$ as input. To calculate the inverse dynamics one can multiply the equation of motion Eq.12 with $\mathbf{B}(\mathbf{q})^{-1}$ to get the control variables $\mathbf{u}$. There are no singular solutions (singular matrix $\mathbf{B}$) possible for this transformation due to the mechanical design.

Control

The control design is done in Matlab Simulink along with the code generation for the target system a dSpace control board. All motion profiles are predefined and tunable with the Control Desk experiment software. The communication between the dSpace system and the hexapod hardware is done via 3 CAN interfaces, each controlling 2 muscles. The CAN interface speed is 1Mbit/s and the cycle time for the controller is 1ms. For the test environment two control schemes are used, a position controller

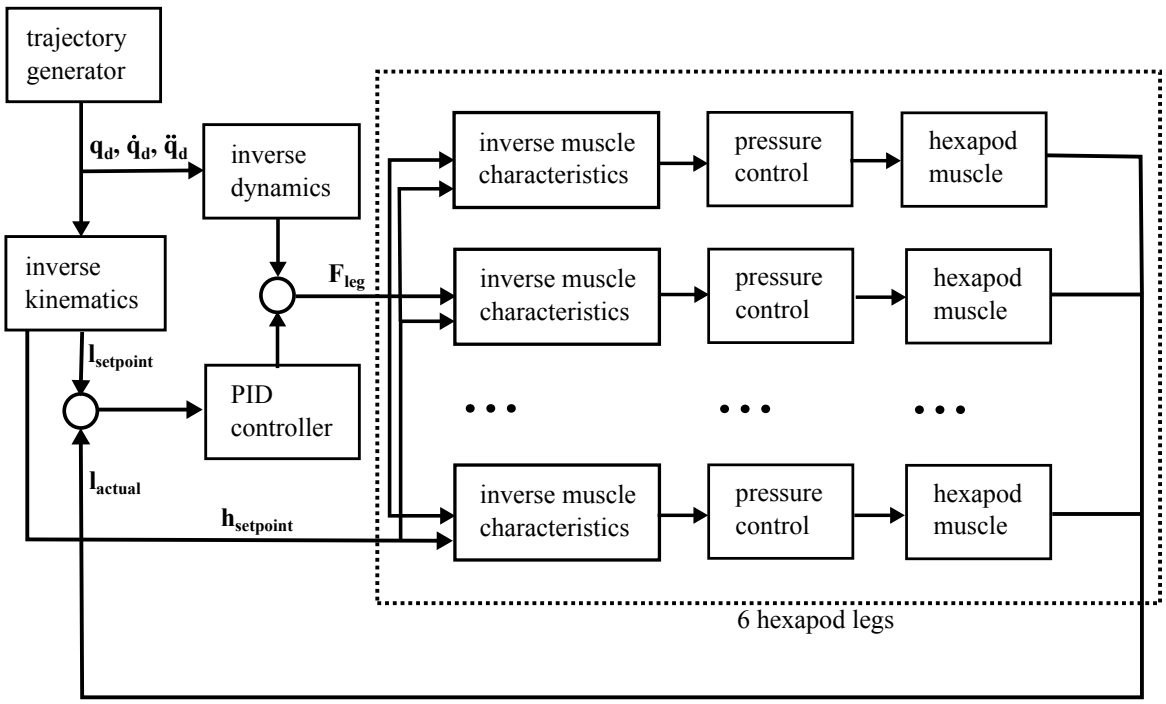

Fig. 4: Control concept for the hexapod

and a pressure controller, see Fig. 4. The position controller is a feed forward (inverse dynamics) with PID control law, and the pressure controller is a PID controller with lookup table to compensate for valve non-linearities. Each leg of the hexapod is driven by pneumatic muscles from FESTO. The

muscle has a non-linear activation characteristic that is compensated by a mathematical model [6]. This model depends on the actual pressure p of the muscle and the contraction level

$$h_i = \frac{l_i}{l_0} 100\%, \tag{14}$$

and can be approximated to

$$F_i = \sum_{j=0}^{4} \left(a_j h_i^j\right) p_i + \sum_{k=0}^{7} \left(b_k h_i^k\right). \tag{15}$$

The pressure control uses mass flow valves and therefore a compensation of the mass flow characteristics together with a PID control law are used. To implement the control laws for position and pressure the following sensors,

- position sensor to measure the length of each leg and therefore the contraction of the muscle,
- pressure sensor for the actual pressure of the muscle,

and actuators,

- FESTO pneumatic muscles with
- mass flow valves,

are used.

Experiment

The experimental implementation and verification using a special designed test mass. It emulates a test object on the hexapod with a mass of 20 kg (mass P), and a second vibrating mass B (500g), attached to it via a spring (flexible beam for the experiment). This mass should be identified by measuring the hexapod position and muscle pressure. For all configurations a spring (steel beam) of dimension 40x3mm with different lengths was used. The maximum spring length is 400mm. The measurements were performed in 3 different configurations.

In configuration 1 the vibrating spring/mass system is tuned to an eigenfrequency of 11 Hz and the mass of 500g is positioned in the center of the hexapod. In configuration 2 the same spring length is used with mass B positioned on the left corner of the hexapod (positive x direction). At last the spring (beam) length is doubled, resulting in a vibration of 6Hz (configuration 3).

The hexapod vibrates vertically (direction z) sweeping slowly from 0 to 18 Hz over a time of 90s. The FFT analysis of the vertical position z, Fig. 5 shows that the Stewart platform oscillates more due to resonance at eigenfrequencies of mass B (6, 11 Hz). Comparing each configuration to configuration 0 one can see an additional oscillation and the vibrating mass is clearly identified by this additional peak.

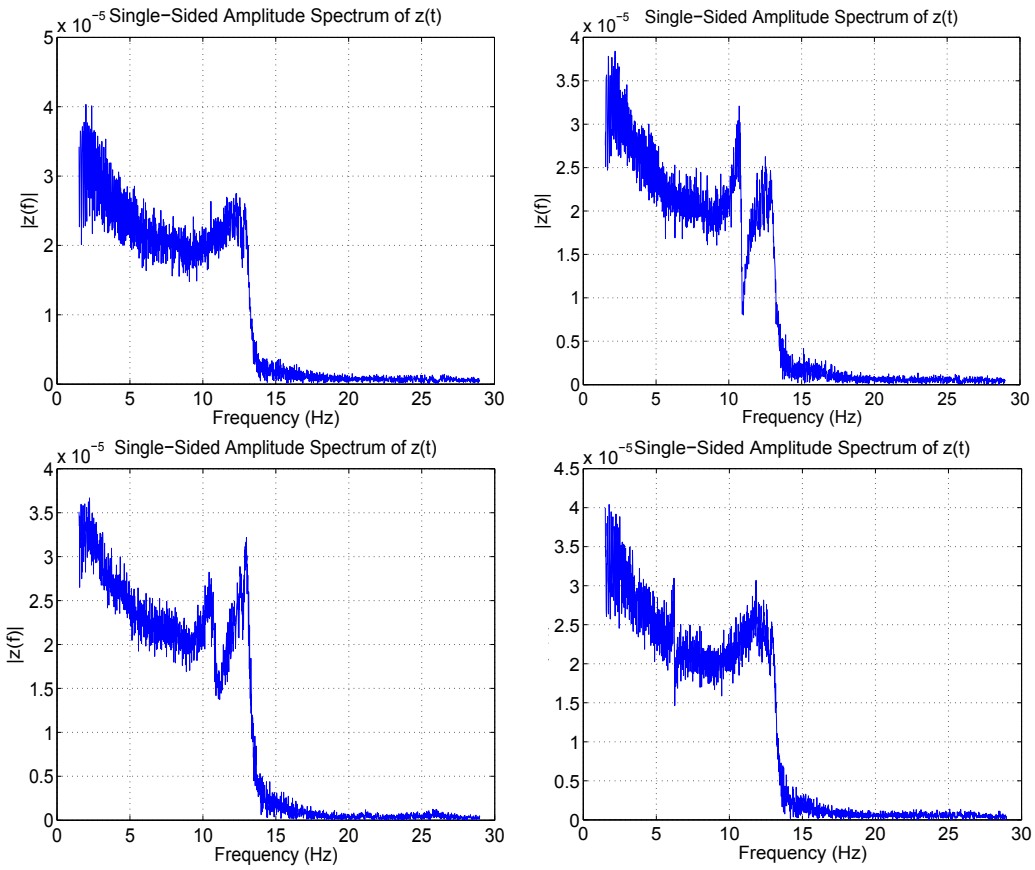

Fig. 5: FFT analysis of position z (upper-left: no loose part config. 0, upper-right: loose part config. 1, lower-left: loose part config. 2, lower-right: loose part config. 3)

Acknowledgment

Support of th present work by the ODEUO (Inner Oscillation Detection and Evaluation of Unknown Test Objects) experiment within the ECHORD (European Clearing House for Open Robotic Development) Project of the European Union and the Austrian Center of Competence in Mechatronics (ACCM) is gratefully acknowledged.

References

[1] H. Aschemann, E. Hofer, Flatnessbased control of a carriage driven by pneumatic muscles, In Proceedings of MMAP (2003) pp. 1219-1224.

[2] J. Merlet, Parallel Robots, Kluwer Academic Publishers, Dordrecht, 2000.

[3] H. Bremer, Elastic Multibody Dynamics-A Direct Ritz Approach, Springer, 2008.

[4] J. Schwandtner, Konstruktion, Modellierung und Regelung eines Hexapods mit Luftmuskel Aktuatorik, JK University Linz, Linz, 2007.

[5] K. Springer, Filter für Bewegungssimulatoren auf Basis einer Stewart-Platform, JK University Linz, Linz, 2010.

[6] R. Neumann, C. Bretz, J. Volzer, Ein Positionierantrieb mit hoher Kraft: Positions- und Druckregelung eines künstlichen pneumatischen Muskels, 4. International Fluidtechnik Kolloquium, 2004.

[7] M.D. Singh, K. Leim, R. Neumann, A. Kecskemethy, Modeling of a pneumatic hybrid actuator using an exponential approach for approximation of the valve-actuator behaviour, In PAMM Proceedings for Applied Mathematics and Mechanics (2006) pp. 803-804.

[8] S. Staicu, Dynamics of the 6-6 Stewart parallel manipulator, Robotics and Computer-Integrated Manufacturing, 27,1, (2011) pp. 212-220.

[9] S. Staicu, Power requirement comparison in the 3-RPR planar parallel robot dynamics, Mechanism and Machine Theory, 44, 5, (2009) pp. 1045-1057.

[10] S. Staicu, Modèle dynamique en robotique, UPB Scientific Bulletin, Series D: Mechanical Engineering,61, 3-4, (1999) pp. 5-19.